RESEARCH PAPER

PCCP
www.rsc.org/pccp

Transition-state-theory calculations for reactions of O(^3P) with halogenated olefins†

Adriana C. Olleta,*[a] Silvia I. Lane*[b] and Sean C. Smith*[a]

[a] *Centre for Computational Molecular Science, Chemistry Building 68, The University of Queensland, Brisbane, Qld 4072, AustraliaE-mail: a.olleta@mailbox.uq.edu.au, s.smith@chemistry.uq.edu.au; Fax: (617) 33654623; Tel: (617) 33657562, (617) 33653975*

[b] *Instituto de Investigaciones en Fisicoquímica de Córdoba (I.N.F.I.Q.C.), Dpto. de Fisicoquímica, Facultad de Ciencias Químicas, Universidad Nacional de Córdoba, Pabellón Argentina, Ciudad Universitaria, Ala 1, Córdoba, 5000, Argentina. E-mail: s-lane@fisquim.fcq.unc.edu.ar; Fax: 54-351-4334188; Tel: 54-351- 4334180/4334169*

Received 25th June 2004, Accepted 18th October 2004
First published as an Advance Article on the web 4th November 2004

The potential energy surfaces for the reactions of atomic oxygen in its ground electronic state, O(^3P), with the olefins: CF_2═CCl_2 and CF_2═CF–CF_3, have been characterized using *ab initio* molecular orbital calculations. Geometry optimization and vibrational frequency calculations were performed for reactants, transition states and products at the MP2 and QCISD levels of theory using the 6-31G(*d*) basis set. This database was then used to calculate the rate constants by means of Transition-State-Theory. To obtain a better reference and to test the reliability of the activation barriers we have also carried out computations using the CCSD(T)(fc)/6-311G†, MP4(SDQ)(fc)/CBSB4 and MP2(fc)/CBSB3 single point energy calculations at both of the above levels of theory, as well as with the composite CBS-RAD procedure (P. M. Mayer, C. J. Parkinson, D. M. Smith and L. Radom, *J. Chem. Phys*., 1998, **108**, 604) and a modification of this approach, called: CBS-RAD(MP2,MP2). It was found that the kinetic parameters obtained in this work particularly with the CBS-RAD (MP2, MP2) procedure are in reasonable agreement with the experimental values. For both reactions it is found that the channels leading to the olefin double-bond addition predominates with respect to any other reaction pathway. However, on account of the different substituents in the alkenes we have located, at all levels of theory, two transition states for each reaction. Moreover, we have found that, for the reactions studied, a correlation exists between the activation energies and the electronic structure of the transition states which can explain the influence of the substituent effect on the reactivity of the halo-olefins.

1 Introduction

The electrophilic addition of the oxygen atom, O(^3P), to halogenated olefins is of interest in the context of chemical oxidative processes in atmospheric and combustion chemistry[1] as well as in understanding the effects of halogen substitution on olefin reactivity. Reactions of the oxygen atom with totally or partially hydrogenated olefins have been studied extensively using different experimental techniques.[2] However, there are only a few studies that have been performed with perhaloalkenes.[3] Cvetanovic[4] has pointed out that in order to explain the observed products, and taking into account the spin conservation rule, in general the reaction of oxygen atoms with olefins will proceed through an electrophilic addition of the oxygen atom to the π bond to form a biradical intermediate of triplet spin. Many theoretical studies have been carried out using *ab initio* molecular orbital calculations for the reactions of totally or partially hydrogenated alkenes with different radicals,[5] oxygen atom, O(^3P),[6] and halogens,[7] the main goal of which was to obtain an accurate characterization of the reaction mechanism. These data point out that the reactivity is greater for olefins having the double bond next to a π-electron system or to an electron-withdrawing substituent.

The absolute rate coefficients for the reactions of O(^3P) with CF_2═CCl_2 and CF_2═CF–CF_3, have been determined at 298 K using a discharge flow system.[8] The aim of the present paper is to assess, using a theoretical approach the effect of the substitution on the activation of the olefinic bond in the addition reaction. To this purpose we have investigated in detail the potential energy surfaces associated with these reactions using second-order Møller–Plesset perturbation theory (MP2), and the QCISD level of theory. The application of *ab initio* methods including dynamic correlation (such as MP2) and a quadratic configuration interaction such as the QCISD method greatly improves the description of the systems under study and provides, for example, barriers in good agreement with experiment. However, the cost of correlated *ab initio* methods is high and increases rapidly with the increasing size of the molecules.

Nevertheless, to obtain better estimates of the reaction energetics we have also used a new procedure called CBS-RAD, together with one modification of this method the CBS-RAD(MP2, MP2), recommended by Mayer *et al.*[9] for the treatment of free radicals. These methods are designed to take

† Electronic supplementary information (ESI) available: Table 1S: Electronic energies and zero-point vibrational energies. Table 2S: Optimized geometry parameters at the various levels of theory here used for reactants, adducts, transition states and products. Table 3S: Optimized frequencies for the reactants, transition states and products. Table 4S: Partition functions (translational, rotational, vibrational, electronic, vibrational corrected for hindered rotation, and hindered rotor). Product of the moments of inertia and the reduced moment of inertia. Hindered rotational barriers, optimized at the various levels of theory, for the species involved in the O(^3P) + CF_2═R addition reactions. See http://www.rsc.org/suppdata/cp/b4/b409689d/

DOI: 10.1039/b409689d

into account the errors that result from spin contamination in open shell systems.

Based on the data obtained from electronic structure calculations, we utilize Transition-State-Theory (TST) to calculate rate coefficients for the addition of the $O(^3P)$ oxygen atom to the named olefins. Finally the derived rate constants of this study are compared with the experimental values recommended by Cvetanovic[2] and those obtained in our laboratory.[8]

2 Computational method

The *ab initio* molecular orbital calculations were performed with the Gaussian 98[10] series of programs. Restricted closed shell wave functions (RMP2 and RQCISD) were used for the various molecules. Unrestricted open shell wave functions (UMP2 and UQCISD) were used for systems such as the oxygen atom, $O(^3P)$, and the carbenes, as well as for the transition states and adducts. All calculations were done within the frozen-core (fc) approximation and with the default optimization criteria. The geometries of the various critical points were fully optimized with the gradient method available in Gaussian 98[10] and the nature of each critical point was characterized by computing the harmonic vibrational frequencies. A vibrational analysis of the transition state structures yielded only one negative eigenvector corresponding to an attack of the oxygen atom on the π bond as the atoms attached to the central carbon are pushed backwards. The addition barriers of the oxygen atom to the halo-olefins as well as the fragmentation barriers were estimated by scanning the O–C and C_1–C_2 bond, respectively. The bond length of O–C or C_1–C_2 was changed by 0.05 Å in each step and the other parameters were optimized. Next, the transition state (TS) calculations were performed to determine the transition structures. The reactants and products of the transition states were confirmed through intrinsic reaction coordinate (IRC) calculations.

To obtain a better estimate of the reaction energetics, we used the CCSD(T)(fc)/6-311G†, MP4(SDQ)(fc)/CBSB4 and MP2(fc)/CBSB3 levels to carry out single-point computations at the geometry calculated with the above mentioned levels of theory.

Furthermore, energies have been improved by using the composite CBS-RAD method and one of the variants of the CBS-RAD procedure: the CBS-RAD(MP2, MP2). The CBS-RAD is a modification of the CBS-Q method in which the geometries and scaled (at 0.9776) zero-point vibrational energy corrections (ZPE), are obtained at the QCISD(fc)/6-31G(*d*) level, and CCSD(T)/6-31+G† single–point energy calculations are used to recover the errors that result from spin-contamination in open-shell systems. The CBS-RAD(MP2, MP2) modification uses geometries and scaled (at 0.9676) MP2(fc)/6-31G(*d*) ZPEs, and is useful for larger systems. The CBS-RAD(MP2, MP2) calculation sequence in this study is performed on the geometry and frequencies determined by an MP2(fc)/6-31G(*d*) calculation; B3-LYP/6-31G(*d*) is the suggested method for frequency calculation with CBS-RAD(MP2,B3-LYP).[9] The total electronic energy and zero point vibrational energies corrections obtained in the geometry and frequency optimizations are reported in Table 1S, ESI.†

The full sequence of calculations required to obtain the total energies by these procedures is described in ref. 9. The atomization energies, ΣD_0, were computed from the calculated energies for the different species and their constituent atoms. Enthalpies of activation, $\Delta H^{\#}$, and formation at 0 K, $\Delta_f H^{\circ}{}_{0\ K}$, were then computed following the method outlined by Nicolaides *et al.*[11] and the experimental heats of formation, $\Delta_f H^{\circ}{}_{0\ K}$, of the constituent elements taken from ref. 12. Standard temperature corrections were applied to $\Delta_f H^{\circ}{}_{0\ K}$, of reactants and products, in order to obtain the enthalpy of formation at 298.15 K, $\Delta_f H^{\circ}{}_{298.15\ K}$.

The rate coefficient, $k(T)$, at temperature T for a bimolecular reaction as a function of the activation energy, E_a, and the pre-exponential factor, $A(T)$, is expressed as: $k(T) = A(T)\exp(-E_a/RT)$. In particular, the A-factor formulation that results from the TST in terms of the partition functions of the reactants and species involved at the transition state is $A(T) = (k_B T/h)\,\kappa[Q^{TS}(T)/Q^{O(^3P)}(T)Q^{CF_2{=}R}(T)]$, where, $Q^{O(^3P)}(T)$, $Q^{CF_2{=}R}(T)$ and $Q^{TS}(T)$, are the total partition functions, at temperature T, of the atomic oxygen in its ground electronic state, the halogenated olefin of the type $CF_2{=}R$ with R = CCl_2 or $CFCF_3$ and transition state, respectively; κ, is the transmission coefficient; k_B is Boltzmann's constant, and h is Planck's constant. The total partition function of all species can be cast in terms of the translational ($Q^X{}_T$), rotational ($Q^X{}_R$), electronic ($Q^X{}_E$), and vibrational ($Q^X{}_V$), partition functions. Vibrational partition functions are evaluated with explicit consideration of the hindered internal rotation of the different tops involved in the halo alkenes and transition state structures, using the method described by Ayala and Schlegel.[13] The evaluation of the electronic partition function, $Q^X{}_E(T)$, for the ground state of the oxygen atom, $O(^3P)$, is a little more complicated than for the other atoms. The lowest state is $^3P_2$, but there are two states very close to it: $^3P_1$, which is 157.4 cm^{-1} above the lowest level and $^3P_0$, which is 226.1 cm^{-1} above the lowest level. Higher states can be neglected at all but highest temperatures. The degenerancies of the three levels are 5, 3 and 1, respectively. Therefore, on computing the electronic partition function for the oxygen atom all these contributions had been taken into account.

3 Results and discussion

A. Reaction mechanism

A complete diagram of the reaction sequence connecting the products and the reactants is given in Fig. 1 for the $O(^3P)/CF_2{=}CCl_2$ case, determined at the MP2/6-31G(*d*) level of theory. We will first examine the addition reaction. In this search, the distance between the attacked carbon and the oxygen atom can be looked upon as the leading parameter of the reaction coordinate; therefore all other parameters were optimized at the various levels of theory here used for a fixed R_{O-C}. Because these reactions exhibit positive temperature dependences in their high-pressure limit rate constants, it appears that the transition state responsible for the observed activation energies must occur quite early in the reaction process, as is shown in Fig. 1 for the specific reaction indicated. This transition state leads to breakage of the π bond and forces hybridization of the carbon atom to change from sp^2 to sp^3. In addition, for this particular process the very exothermic transformation to the adduct [O–CF_2–CCl_2], occurs rapidly and does not influence

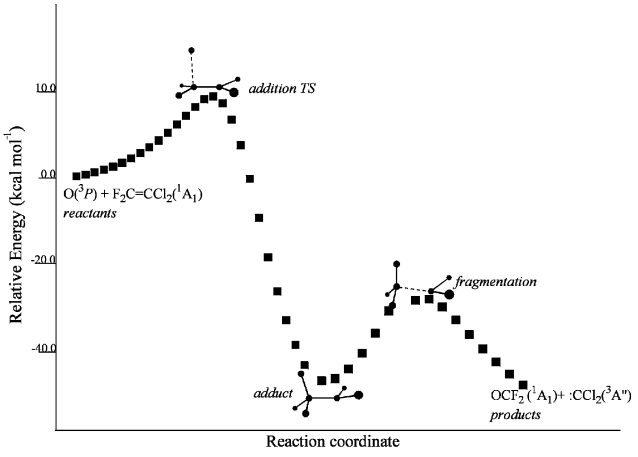

Fig. 1 Energy profile for the reaction of: $O(^3P)$ + $CF_2{=}CCl_2$ obtained at the MP2/6-31G(*d*) level of theory.

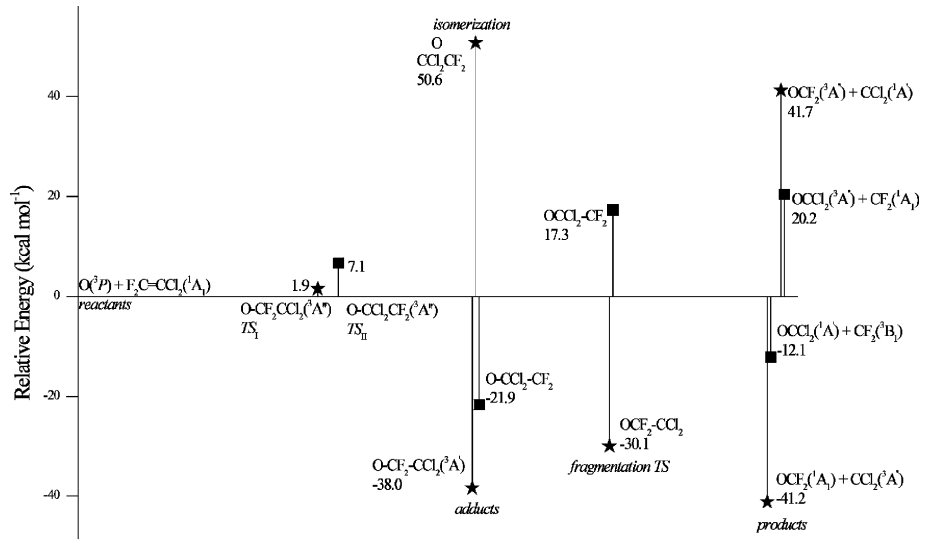

Fig. 2 Potential energy surface for the reaction of: $O(^3P) + CF_2{=}CCl_2$, calculated at the CBS-RAD(MP2, MP2) level of theory. The star (★) indicates the addition to C_1 and the square to C_2 (■).

the overall rate of addition. In this adduct the oxygen atom is localized on one of the two double-bond carbon atoms forming a triplet biradical.

On the other hand, the formation of the final products from the intermediate adduct involves a (C–C) fragmentation proceeding *via* a second transition state located at a barrier in the exit channel of the potential energy surface. In the reactions studied herein we have found that the exit channel barrier is much lower in energy than the entrance channel barrier, similar to the case shown in Fig. 1 (see the results below for specific details). This has two corollaries: firstly the micro canonical rate constants for dissociation of the adduct to products will be large due to the excess energy involved, with the consequence that the lifetime of the metastable adduct is sufficiently short that collisional relaxation can be neglected. This is the origin of the experimentally observed pressure independence of these reactions. Secondly, upon formation of the adduct the branching fraction for dissociation forward to products (*vs.* reverse dissociation to reactants) will be essentially unity such that the effective rate determining step in the reaction is passage through the entrance channel transition state. Hence, in our kinetic analysis below we can model the overall reaction kinetics by simply computing the thermal rate constant for passage through the entrance channel transition state using Canonical-Transition-State-Theory, and a full Rice–Ramsperger–Kassel–Marcus (RRKM) theory analysis of branching ratios is not required for the present study. Furthermore, in order to verify the proposed mechanism, we have performed calculations for the two possible addition channels (addition to C_1 or C_2) as well as for the isomerization barrier between the two resulting adducts of the addition reaction (Figs. 2 and 3).

B. Structures

Table 1 lists the essential structural parameters calculated with the 6-31G(*d*) basis set, at the different levels of theory, of the reactants, transition state structures and adducts located for the electrophilic addition of the oxygen atom, $O(^3P)$ to the halogenated olefins: $O(^3P) + CF_2{=}R$, where $R = CCl_2$ or $CF–CF_3$. All other structural parameters as well as those for the final products, and experimental values, are reported in Tables 2S–4S, ESI.† The most relevant geometric parameters given in these Tables are defined in Fig. 4 for the transition state structures: TS_I ($O–CF_2CCl_2$), TS_{II} ($O–CCl_2CF_2$), TS_{III} ($O–CF_2CFCF_3$) and TS_{IV} ($CF_2O–CFCF_3$). We discuss first the

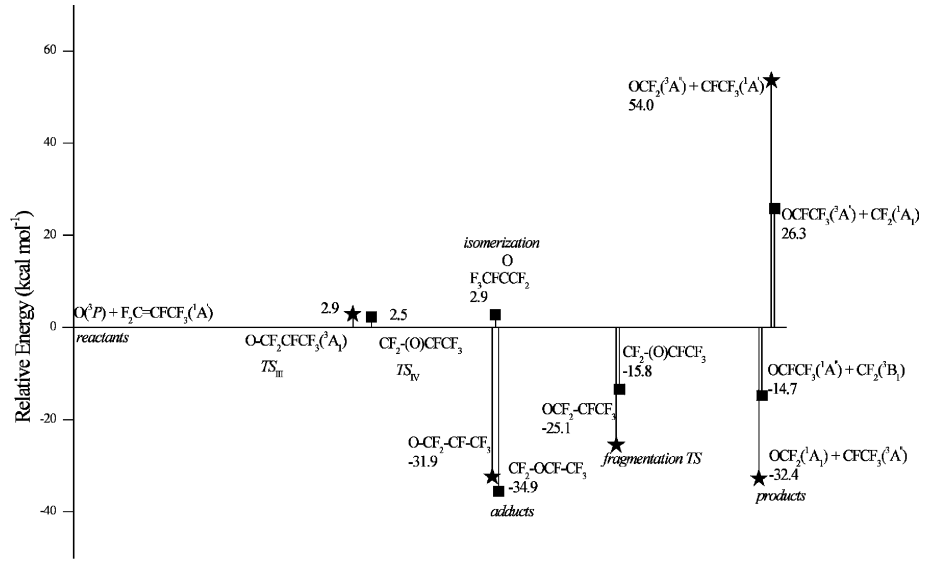

Fig. 3 Potential energy surface for the reaction of: $O(^3P) + CF_2{=}CFCF_3$, calculated at the CBS-RAD(MP2, MP2) level of theory. The star (★) indicates the addition to C_1 and the square to C_2 (■).

Table 1 Essential parameters for reactants, transition states and adducts involved in $O(^3P)$ atom addition reactions to the CF_2═R, with R = CCl_2 or $CFCF_3$, halogenated olefins obtained with the 6-31G(*d*) basis set at various levels of theory[a]

QCISD/	*a*	*b*	α	ε	φ	ν^{*b}	$\nu^{\#b}$	$V_0{}^c$
CF_2═CCl_2	1.336	∞	—	180.0	180.0			
TS_I	1.362	2.064	93.55	160.0	173.3	607	93	19.7
$Adduct_IOCF_2CCl_2$	1.504	1.422	110.4	120.4	158.4		36	2.7
TS_{II}	1.380	1.964	100.6	146.6	163.9	686	111	14.3
$Adduct_{II}OCCl_2CF_2$	1.522	1.382	108.8	118.4	129.0		47	3.2
$IsomerizationTS_{I–II}$	1.296	2.040	98.82	160.4	175.4	607	—	—
Fragmentation TS_I	1.912	1.232	95.66	107.5	162.9	688	27	1.6
Fragmentation TS_{II}	2.081	1.371	110.0	117.2	129.9	556	18	0.5
CF_2═$CFCF_3$	1.331	∞	—	180.0	180.0		33	1.5
TS_{III}	1.370	2.038	96.66	155.1	159.8	702	37	2.0
$Adduct_{III}OCF_2CFCF_3$	1.504	1.379	113.9	118.7	144.3	—	37	17.4
							43	2.6
TS_{IV}	1.362	2.010	100.5	151.2	169.5	551	43	1.9
$Adduct_{IV}CF_2OCFCF_3$	1.529	1.344	107.6	116.8	130.9		35	8.5
							92	7.5
Isomerization $TS_{III–IV}$	1.362	2.038	93.20	159.2	168.1	625	30	18.2
Fragmentation TS_{III}	1.981	1.221	94.70	102.8	132.3	639	28	1.1
Fragmentation TS_{IV}	2.162	1.213	93.92	99.72	127.0	674	25	4.6
MP2/								
CF_2═CCl_2	1.337	∞	—	180.0	180.0			
TS_I	1.342	1.976	92.49	162.0	175.2	881	108	25.4
$Adduct_1OCF_2CCl_2$	1.513	1.372	110.8	118.8	152.4		38	3.1
TS_{II}	1.358	1.921	101.3	147.6	170.2	829	120	16.4
$Adduct_{II}OCCl_2CF_2$	1.525	1.375	107.9	119.1	128.0		46	3.0
$IsomerizationTS_{I–II}$	1.477	3.094	80.07	131.0	150.1	43	—	—
Fragmentation TS_I	1.834	1.218	100.3	103.2	150.3		46	4.7
Fragmentation TS_{II}	2.681	1.340	103.1	118.5	96.38		13	0.3
CF_2═$CFCF_3$	1.335	∞	—	180.0	180.0		33	1.5
TS_{III}	1.343	1.958	91.90	161.6	172.3	882	31	1.4
$Adduct_{III}OCF_2CFCF_3$	1.502	1.380	113.8	118.8	143.5	—	37	17.8
							45	2.9
TS_{IV}	1.341	1.947	100.4	152.7	173.0	736	55	2.8
$Adduct_{IV}CF_2OCFCF_3$	1.525	1.345	107.5	117.0	130.7	—	35	8.2
							93	7.6
$IsomerizationTS_{III–IV}$	1.343	1.958	91.92	161.6	172.3	892	31	1.4
Fragmentation TS_{III}	2.064	1.212	94.37	101.2	133.3	857	35	1.7
Fragmentation TS_{IV}	2.052	1.197	92.32	100.9	125.6	416	25	4.4

[a] Bond lengths, *a* and *b*, are in angstroms; bond angles α and dihedral angles, ε and φ, are in degrees. [b] ν^* and $\nu^\#$ in cm^{-1} are the imaginary frequencies and the frequencies associated with the hindered rotation, respectively. [c] Hindered rotational barriers V_0, in kcal mol^{-1}.

MP2 results and analyze the geometrical modifications found with the other level of theory.

We begin our discussion with the results obtained for the CF_2═CCl_2. In this case we have located two transition states, TS_I and TS_{II}, both characterized by C_s symmetry. TS_I and TS_{II} lead to the addition of the $O(^3P)$ atom to the olefin double bond at the C_1 and C_2 carbon atoms, respectively, and in both cases the transition vector corresponding to the imaginary frequency is dominated by the approaching distance (*b*). At this level of theory the forming O–C and the breaking C═C double bond lengths are 1.976 and 1.342 Å for TS_I and 1.921 and 1.358 Å for TS_{II}, respectively, while the angle of attack of the oxygen atom to the halogenated olefin is 92.49 and 101.3° for TS_I and TS_{II}, respectively. As a consequence of the formation of the new O–C_1 or O–C_2 bond a considerable rehybridization of the olefin carbon atom takes place. A measure of the pyramidalization of the considered carbon atom C_1 or C_2, is given by the angle ε which is 162.0 and 147.6° for the TS_I and TS_{II}, respectively (ε, is represented in Fig. 4 and corresponds to the angle between the C–C bond and the FC_1F or ClC_2Cl plane, its value is 180° in the planar olefin). The two substituents bonded to the other carbon atom are bent out of the olefin molecular plane, but in the opposite direction with respect to the attacked carbon atom. The pyramidalization in this latter carbon is described by the φ angle (also defined in Fig. 4) which is: 175.2 and 170.2° for the transition states, I, and II, respectively.

For the reaction between $O(^3P)$ and perfluoropropene, even though the TS_{III} has lost the C_s symmetry, it is very similar to the analogue transition states discussed in the case of CF_2═CCl_2. In this structure the angle of attack of the oxygen atom is α = 91.90° the new forming bond length O–C_1 is 1.958 Å and the C_1–C_2 bond length is 1.343 Å. Similarly, in this case a significant rehybridization of the C_1 atom takes place (the ε angle is 161.6°) and the incipient carbon-radical center is slightly pyramidal (the φ angle is 172.3°). TS_{IV} is characterized by similar to TS_{III} bond length values of the two bonds involved in the reaction: O–C_2 is 1.947 Å, and the C_1–C_2 bond is 1.341 Å. The steric repulsion between the oxygen atom and the trifluoromethyl group is probably responsible for a greater value than in TS_{III} of the angle of attack, which becomes 100.4°. The results show, furthermore, the optimum structure found for the triplet biradical adducts OCF_2–R (with R = CCl_2 or $CFCF_3$) and $OCCl_2CF_2$ and CF_2OCFCF_3. In these structures, shortening of the new O–C_1 or O–C_2 bond, which becomes complete is found and also a further lengthening of

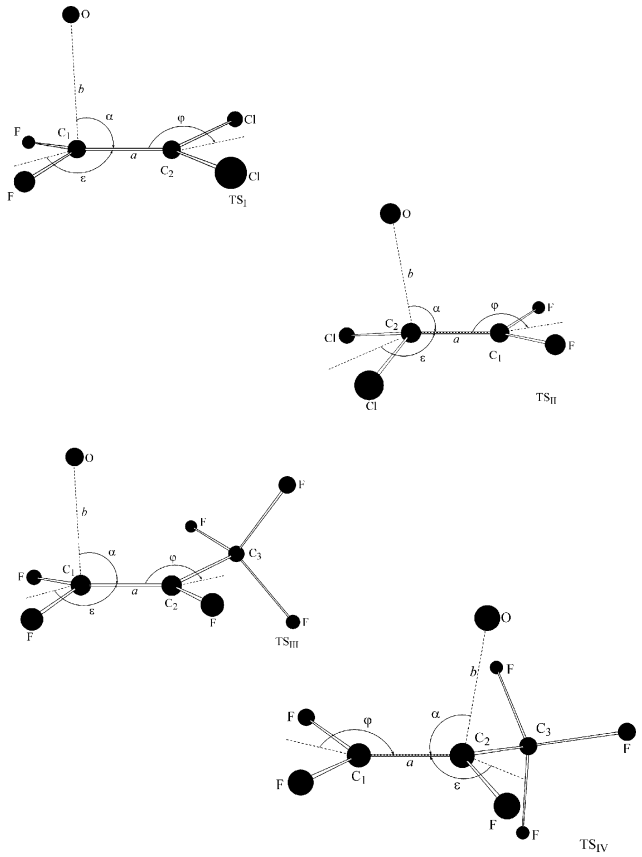

Fig. 4 Schematic representation of the transition structures: TS_I (O–CF_2CCl_2); TS_{II} (O–CCl_2CF_2); TS_{III} (O–CF_2CFCF_3) and TS_{IV} (CF_2–(O)$CFCF_3$).

the C_1–C_2 bond which manifestly loses its double bond character. TS_{III} and TS_{IV} lead to the triplet biradical adducts $Adduct_{III}$ and $Adduct_{IV}$, respectively. The lengths of the O–C and C–C bonds are similar in the two molecules, while the $\alpha(OC_1C_2)$ angle is smaller in $Adduct_{IV}$ than in $Adduct_{III}$. A more significant difference in the comparison between the two biradicals is found in the C_2–C_3 bond distance which is 1.502 Å in $Adduct_{III}$ and 1.525 Å in $Adduct_{IV}$. The smaller value in $Adduct_{III}$ has probably the effect of maximizing the attractive interaction between the singly occupied orbital centered on C_2 and the empty σ(C–F*) orbital associated with the C–F bond, orthogonal to the molecular plane.

On considering these two possible channels (addition to C_1 or C_2) we have calculated the barrier for the isomerization between the two adducts for each reaction. In the case of the addition reaction of $O(^3P)$ to the CF_2=CCl_2 the isomerization barrier is too high to be taken into account. This result indicates that the addition reaction is that in which the oxygen atom adds to the fluorine substituted carbon atom, which is in agreement with the experimental evidence that F_2CO is the predominant product.[14] In the case of the perfluoropropene the experimental results show evidence of two different oxygen-containing products, F_2CO and F_3CFCO. The formation of these two products can be explained taking into account that the activation barriers are similar, whereas the isomerization barrier between the two adducts is rather high in comparison with the fragmentation barriers leading to products.

For these reactions the eigenvector corresponding to the imaginary frequency was observed to be primarily dominated by the approaching distance O–C_1. The absolute values of the imaginary frequencies associated with these transition vectors are also reported in Table 1.

Direct inspection of the low frequency modes for the CF_2CFCF_3 and corresponding transition state indicates that those modes correspond to an internal rotation of the CF_3 group about the CF_2=CF fragment for the CF_2CFCF_3 or about the O–CF_2–CF group in the case of the TS_{III} transition state, for example. Given that the barriers for these rotations are sufficiently small; these modes were treated as hindered rotors instead of harmonic vibrations. Thus, these modes were modelled with a hindered rotor partition function, $Q_{HR}(T)$, calculated by the method devised by Ayala and Schlegel[13] in the expression of the rate constant. Assuming a harmonic potential near the bottom of the well, the rotational barriers of each of the structures corresponding to the transition states and halogenated propene were calculated as, $V_o = 8\pi^2(\nu^{\#})^2 I_R/\sigma^2$, where $\nu^{\#}$ represents the frequency associated with the hindered internal rotation, I_R the reduced moments of inertia involving the tops related to the internal rotation and σ the periodicity of the potential. The characteristic low frequencies and the derived rotational barriers are also shown in Table 1.

C. Reaction enthalpies

The accurate prediction of the reaction enthalpies and kinetic parameters of addition reactions is a difficult problem, and it is well-known that high levels of theory are needed to reproduce the experimental values. In the following we discuss the computed energy results and compare them with the available experimental values. The reaction enthalpy for a given reaction represents the difference between the enthalpy of formation of the formed O–C bond and the broken C_1–C_2 double bond of the halogenated olefin. Thus, for each of the species involved in the title reactions we have determined the enthalpy of formation and from these values the corresponding reaction enthalpies. The calculated and experimental values (if available) for the enthalpies of formation and reaction enthalpies are listed in Table 2. However, it should be noted that the experimental $\Delta_f H_{298.15\ K}$ values on account of their wide spread make a direct comparison difficult. Therefore, among the experimental enthalpies of formation of the species involved we choose the most reliable values from our viewpoint and used them as reference values. On the other hand, the existing experimental data on halogen compounds are relatively imprecise especially for fluorine and chlorine compounds in comparison to hydrocarbons and there is a lack of information for some of the species involved in the reactions here studied. Nevertheless, there is in general an acceptable agreement between the available experimental values for the enthalpies of formation and both levels of theory here used.

D. Reaction barriers

Table 3 shows the computed vibrationally adiabatic barriers, VAB, for the reactions under study. These barriers were determined using the following equation: $VAB = E_{TS} - E_R + ZPE_{TS} - ZPE_R$, where E_{TS} and E_R are the *ab initio* energies of the transition state and reactants, respectively while ZPE_{TS} and ZPE_R are the corresponding zero point energy corrections. The obtained results, reinforce the experimental evidence that CF_2 is, at most, only a very minor product from CF_2=CCl_2. At all levels of theory here used the addition reaction oriented to C_1 is highly favoured.

On the other hand, the reaction of C_3F_6 with oxygen atoms is a bit more complex. The oxygen atom can react with C_3F_6 in two ways:

$$O(^3P) + C_3F_6 \rightarrow CF_2O + CF_3CF \quad (a)$$

$$\rightarrow CF_3CFO + CF_2 \quad (b)$$

where, CF_2 and CF_3CF are in their triplet states, as expected from the spin conservation rule. In agreement with the experimental observations, most all of the levels of theory here used, indicate that reaction (a) is the main channel.

Table 2 Calculated and experimental, enthalpy of formation, $\Delta_f H_{298.15\ K}$ and enthalpy of reaction, $\Delta_r H_{298.15\ K}$, in kcal mol^{-1}[a]

		CBS-RAD (QCISD,QCISD)	CBS-RAD (MP2, MP2)	Exp.[a]	Ref.
CF_2=CCl_2	$^1A_1$	−81.0	−81.3	***−80.2 ± 1.0***	15
CF_2=$CFCF_3$	$^1A_1$	−277.9	−277.9	***275.3 ± 0.1***	16
CF_2	$^1A_1$	−48.0	−44.2	***−43.5 ± 1.5***	17
				−41.1 ± 2.0	18
				−49 ± 3.0	19
				−39.4 ± 3.4	20
				−40.9 ± 2.4	21
				−46.4 ± 2.2	22
CF_2	$^3B_1$	12.3	12.3	***12.7 ± 0.1***	23
CCl_2	$^1A_1$	53.2	52.9	***57.0 ± 5.0***	17
				39. ± 3.	20
				52.1 ± 3.4	21
				55. ± 2.	24
				51.0 ± 2.0	25
				57.2 ± 4.0	26
				57.12	27
CCl_2	$^3B_1$	73.7	73.7		
$CFCF_3$	$^1A_1$	−123.2	−123.2	***−140 ± 3***	28
$CFCF_3$	$^3B_1$	−106.6	−106.1		
OCF_2	$^1A_1$	−145.1	−145.0	*−152.7 ± 0.4*	17
				−153.1 ± 1.4	29
				−145.6 ± 1.0	30
OCF_2	$^3B_1$	−41.1	−41.2		
$OCCl_2$	$^1A_1$	−54.3	−54.3	***−52.60 ± 0.8***	17
				−52.50 ± 0.22	31
				−52.37 ± 0.14	32
				−50.07 ± 0.28	33
				−52.1 ± 3.4	21
$OCCl_2$	$^3B_1$	35.6	40.0		
$OCFCF_3$	$^1A_1$	−245.4	−245.4		
$OCFCF_3$	$^3B_1$	−147.7	−147.8		
$O(^3P)$ + CF_2=$CCl_2(^1A_1)$ → $OCF_2(^1A_1)$ + $:CCl_2(^3B_1)$		−49.9	−48.7		
$O(^3P)$ + CF_2=$CCl_2(^1A_1)$ → $OCCl_2(^1A_1)$ + $:CF_2(^3B_1)$		−20.5	−19.4	*−18.8 ± 2.5*	
$O(^3P)$ + CF_2=$CCl_2(^1A_1)$ → $OCF_2(^3A'')$ + $:CCl_2(^{1a}{}_1)$		33.6	34.3		
$O(^3P)$ + CF_2=$CCl_2(^1A_1)$ → $OCCl_2(^3A'')$ + $:CF_2(^1A_1)$		9.1	18.4		
$O(^3P)$ + CF_2=$CFCF_3(^1A_1)$ → $OCF_2(^1A_1)$ + $:CFCF_3(^3B_1)$		−33.4	−32.3		
$O(^3P)$ + CF_2=$CFCF_3(^1A_1)$ → $:CF_2(^1A_1)$ + $OCFCF_3(^3A')$		22.6	26.8		
$O(^3P)$ + CF_2=$CFCF_3(^1A_1)$ → $OCF_2(^3A'')$ + $:CFCF_3(^1A')$		54.0	54.4		
$O(^3P)$ + CF_2=$CFCF_3(^1A_1)$ → $:CF_2(^3B_1)$ + $OCFCF_3(^1A')$		−14.8	−14.3		

[a] When several experimental $\Delta_f H_{298.15\ K}$ values had been reported, we choose the most reliable of them (highlighted in bold-italic) and used it in the subsequent calculations as a reference value.

E. Kinetic parameters

Table 4 lists the Arrhenius A factor and activation energy E_a values obtained from fitting of the rate constants computed over the temperature range at which these reactions were experimentally determined. Table 4 also shows the computed absolute rate constants at 298 K and the experimental values recommended in the literature and those determined in our laboratory. Inspection of Table 4 shows that the CBS-RAD(MP2, MP2) level provides for the addition of oxygen atoms to CF_2=CCl_2 an activation energy of 1.9 kcal mol^{-1} in quite good agreement with the experimental value of about 1.3 kcal mol^{-1}. We must point out, however, that the CBS-RAD procedure tends to overestimate the activation energy. In the case of the addition reaction to the perfluoropropene, it was experimentally found that the ratio of the rate constants

Table 3 Calculated vibrationally adiabatic barriers, VAB, in kcal mol^{-1}

VAB	O–CF_2CCl_2	O–CCl_2CF_2	O–CF_2CFCF_3	CF_2–$OCFCF_3$
CBS-RAD	2.76	7.43	5.67	3.13
CCSD(T)/6-31+G(d)//QCISD/6-31G(*d*)	2.26	6.38	5.95	7.80
MP4(SDQ)/CBSB4//QCISD/6-31G(*d*)	9.94	15.24	13.93	15.61
MP2/CBSB3//QCISD/6-31G(*d*)	13.38	19.30	17.46	16.91
QCISD/6-31G(*d*)	5.17	12.50	9.02	9.05
CBS-RAD (MP2, MP2)	1.87	7.23	2.92	2.54
CCSD(T)/6-31+G(d)//MP2/6-31G(*d*)	3.06	6.95	5.84	8.77
MP4(SDQ)/CBSB4//MP2/6-31G(*d*)	10.60	15.14	12.62	15.93
MP2/CBSB3//MP2/6-31G(*d*)	12.38	17.76	13.90	15.52
PMP2/6-31G(*d*)	6.25	12.94	7.15	7.47

Table 4 Summary of the kinetic parameters calculated with the CBS-RAD and CBS-RAD(MP2, MP2) procedures

	Temp. range/K	E_a/kcal mol^{-1}	A/cm^3 mol^{-1} s^{-1}	$k_{(298\ K)}$
$O(^3P) + CF_2{=}CCl_2$				
CBS-RAD				
TS_I		2.8	3.9×10^{12}	3.2×10^{10}
TS_{II}		7.5	2.3×10^{12}	7.2×10^{6}
CBS-RAD(MP2, MP2)				
TS_I		1.9	2.5×10^{12}	2.4×10^{11}
TS_{II}		7.1	1.7×10^{12}	2.2×10^{8}
(Experimental)	(290–450)	*1.31 ± 0.20*[a]	*3.5 × 10*^{12} [a]	*3.9 × 10*^{11}[a]
				(1.90 ± 0.40) × 10^{11} [b]
$O(^3P) + CF_2{=}CFCF_3$				
CBS-RAD				
TS_{III}		5.6	1.9×10^{11}	1.4×10^{7}
TS_{IV}		3.1	2.6×10^{12}	1.3×10^{10}
CBS-RAD(MP2, MP2)				
TS_{III}		2.9	1.4×10^{11}	1.0×10^{9}
TS_{IV}		2.5	9.8×10^{10}	1.3×10^{9}
(Experimental)	(297–398)	*2.32 ± 0.38*[a]	*7.8 × 10*^{11} [a]	*1.5 × 10*^{10} [a]
				(1.81 ± 0.60) × 10^{10} [b]

[a] Ref. 2. [b] Ref. 8.

determined from the ratio of the quantum yields is about 6.5. However, in our calculation we have failed to find such a ratio even when the values for the activation energy and A factor compare quite well with the experimental value, probably because some deficiencies in the methodology related with spin contamination and electron correlation in perfluorinated systems.

F. Reactivity trends

We have examined the polarity changes of the reactive C_1–C_2 bond in an attempt to interpret the factors that probably determine the reactivity of the halogenated olefins. If the polarity (p) of a C_1–C_2 bond in the olefin is defined as the net charge difference (q) between the two atoms involved, $p(C_1–C_2) = qC_1 - qC_2$, then the polarity variation of a reactive bond could be expressed as, $\Delta p(C_1–C_2) = p^*(C_1–C_2)$ (TS) $- p(C_1–C_2)$ (reactant), where $p^*(C_1–C_2)$ (TS) and $p(C_1–C_2)$ (reactant) are the polarities at the transition state and at the reactant, respectively. The electron transfer from the R fragment (with $R = CCl_2$ or $CFCF_3$) toward the reactive C_1 atom is well reflected by these polarity changes. In our calculations the charges were computed by using the Mulliken population analysis. Even though the charge is not a quantum mechanical observable and this partitioning of the charge is necessarily arbitrary, we decided to explain the differences in reactivity of the halogenated olefins toward the $O(^3P)$ attack by analyzing the polarity variation with the ionization potential of the olefin and also with the activation energy (Table 5). For a large number of small radical/molecule systems, activation energies within homologous series have shown to correlate quantitatively with the electron donating and electron accepting abilities of the reactants. In this manner we have confidence that frontier orbital analysis can be used to examine the character of the rate determining transition state. For the halogenated propene studied in this work, the highest occupied molecular orbital is composed of carbon–carbon π-bonding and halogen atom lone pair contributions. The attacking $O(^3P)$ experiences greater nonbonding interactions in the transition state than it does in the $O(^3P)$/alkenes reactions where the HOMO is solely carbon–carbon π bonding. In addition, the electron density originally localized in the alkene π bond is more delocalized in the halogenated olefin, particularly in the lowest lying valence π orbital which is bonding between the carbon and halogen substituents. As a result, the rate constants for these reactions do not correlate in a simple manner with the energy of the HOMO (the experimental ionization potential), as is the case in the $O(^3P)$/alkenes reactions, and the rate constants are suppressed relative to the $O(^3P)$/alkenes trend by a barrier for $O(^3P)$ insertion into the carbon–carbon π bond. For the halogenated ethylenes a similar trend to that observed for the halopropenes could be expected, however when the chlorine atom is the substituent, it is necessary to consider not only the withdrawal electron effect, but also an increase of the electron density of the π bond due to the mesomeric effect, M^+, which enhances the olefin's reactivity towards the electrophilic attack by the oxygen atom.

Table 5 Polarities variation ($\Delta p(C_1–C_2)$), ionization potentials (IP, eV), and activation energies (E_a, kcal mol^{-1})

	$\Delta p(C_1–C_2)$	IP	E_a
$CF_2{=}CCl_2$	0.188	9.76	1.51
$CF_2{=}CFCF_3$	0.159	11.52	2.90

Conclusions

In this paper, we have investigated the potential energy surfaces associated with the addition reactions of the oxygen atom $O(^3P)$ to $CF_2{=}CCl_2$, and $CF_2{=}CF–CF_3$, using MP2 and QCISD levels of theory with the 6-31G(d) basis set. At all levels of theory we have determined for each of the reactions studied that in the first step the reaction proceeds through a transition state that consists on the addition of the oxygen atom to the double bond, followed by a rearrangement to yield a stabilized adduct. This intermediate was visualized as a triplet biradical which undergoes a C_1–C_2 pressure-independent fragmentation. This general scheme gives support to the experimental findings. In addition, the CBS-RAD procedure and the proposed modification of this called CBS-RAD(MP2, MP2), were applied to compute the $\Delta_f H^o_{298.15\ K}$, for molecules and carbenes and from the resulting values the reaction enthalpies $\Delta_r H^o_{298.15\ K}$, as well as to determine the kinetic parameters of the series studied.

Finally we have found some mechanistic details for these reactions, the fact that the attack of the oxygen atom to the C_1 in the olefin is highly favored, could be explained taking into account that several effects compete in this process: (a) the electronic density of the σ bond in the C=C bond, is reduced

by the inductive effect of the halogen atom. (b) Steric hindrance, due to the presence of the CF_3 group and Cl atoms in the olefin makes attack on the substituted carbon more difficult, and favors the attack on the less substituted carbon.

There are many studies of O atom reactions with a variety of unsaturated hydrocarbons, but only limited information is available for halogenated alkenes. From the available data it should be indicated that the trend in the rate constants appears to be entirely related to the variations in the activation energies. In general Cvetanovic[4] has indicated that on account of the electrophilic trend of the rates it is probable that the lowering of the potential energy can be explained, by partial charge transfer from the olefin to the attacking oxygen atom in the transition state. The initial repulsion is responsible for the existence of potential barriers.

Particularly from the rate constants values for the reactions of $O(^3P)$ with related hydro- and halo-alkenes it is observed that the presence of F atoms or CF_3 group in the olefin produces significant decrease of its reactivity towards the $O(^3P)$ atoms. This effect can be attributed to the strong electron-withdrawing capacity of the F and the CF_3 radicals which reduces the charge density on the atom carbon next to the double bond as well as the polarizability of the π electrons, leading to a decrease of the rate constants consistent with the electrophilic character of the $O(^3P)$ atom.

Using our energetical results, the rate constants calculated at room temperature, are in good agreement with the experimental values measured in the same conditions.

Acknowledgements

The authors wish to thank Dr Joan Bertran Rusca for helpful discussions. We gratefully acknowledge financial support from the Australian Research Council (Discovery Project Grant No. DP0211019), CONICET (Argentina), ANPCyT (Contrato de Prestámo BID 1201/OC-AR) Agencia Córdoba Ciencia and SECyT-UNC (Córdoba, Argentina). We thank the University of Queensland and the Queensland Parallel Supercomputing Foundation for allocation of high performance computing resources.

References

1 R. P. Wayne, *Chemistry of Atmospheres*, Oxford Science Publication Inc., Oxford, 2nd edn., 1991.
2 R. J. Cvetanovic, *J. Phys. Chem. Ref. Data*, 1987, **16**, 261.
3 (*a*) S. Koda, *J. Phys. Chem*., 1979, **83**, 2065; (*b*) W. J. R. Tyerman, *Trans. Faraday Soc*., 1969, **65**, 163; (*c*) D. Saunders and J. Heicklen, *J. Phys. Chem*., 1966, **70**, 1950; (*d*) D. Saunders and J. Heicklen, *J. Am. Chem. Soc*., 1965, **87**, 4062; (*e*) R. C. Mitchell and J. P. Simons, *J. Chem. Soc. B*, 1968, 1005; (*f*) N. Cohen and J. Heicklen, *J. Phys. Chem*., 1966, **70**(10), 3082; (*g*) S. Y. Leeand, H. S. Yoo, W. K. Kang and K.-H. Jung, *Chem. Phys. Lett*., 1996, **257**, 415.
4 R. J. Cvetanovic, *Adv. Photochem*., 1963, **1**, 115.
5 (*a*) K. N. Houk, M. N. Paddon-Row, D. C. Spellmeyer, N. G. Rondan and S. Nagase, *J. Org. Chem*., 1986, **51**, 2874; (*b*) R. Arnaud, R. Subra, V. Barone, F. Lelj, S. Olivella, A. Sole and N. Russo, *J. Chem. Soc., Perkin Trans. 2*, 1986, 1517; (*c*) T. Clark, *J. Chem. Soc., Chem. Commun*., 1986, 1774; (*d*) T. Fueno and M. Kamachi, *Macromolecules*, 1988, **21**, 908; (*e*) C. Gonzales, C. Sosa and H. B. Schlegel, *J. Phys. Chem*., 1989, **93**, 2435; (*f*) C. Gonzales, C. Sosa and H. B. Schlegel, *J. Phys. Chem*., 1989, **93**, 8388; (*g*) R. Arnaud, *New J. Chem*., 1989, **13**, 543; (*h*) H. Zipse, J. He, K. N. Houk and B. Giese, *J. Am. Chem. Soc*., 1991, **113**, 4324; (*i*) R. Arnaud and S. Vidal, *New J. Chem*., 1992, **16**, 471; (*j*) D. J. Tozer, J. S. Andrews, R. D. Amos and N. C. Handy, *Chem. Phys. Lett*., 1992, **199**, 229; (*k*) C. Schmidt, M. Warken and N. C. Handy, *Chem. Phys. Lett*., 1993, **211**, 272; (*l*) T. P. Davis and S. C. Rogers, *Macromol. Theory Simul*., 1994, **3**, 905; (*m*) V. Barone and M. Orlandini, *Chem. Phys. Lett*., 1995, **246**, 45; (*n*) A. Bottoni, *J. Chem. Soc., Perkin Trans. 2*, 1996, 2041; (*o*) A. Bottoni, *J. Phys. Chem. A*, 1997, **101**, 4402; (*p*) B. J. Jursic, *Chem. Soc., Perkin. Trans. 2*, 1997, 637; (*q*) M. W. Wong, A. Pross and L. Radom, *J. Am. Chem. Soc*., 1993, **115**, 11050; (*r*) M. W. Wong, A. Pross and L. Radom, *Isr. J. Chem*., 1993, **33**, 415; (*s*) M. W. Wong, A. Pross and L. Radom, *J. Am. Chem. Soc*., 1994, **116**, 6284; (*t*) M. W. Wong, A. Pross and L. Radom, *J. Chem. Soc*., 1994, **116**, 11938; (*u*) M. W. Wong and L. Radom, *J. Phys. Chem*., 1995, **99**, 8582; (*v*) J. P. A. Heutz, R. G. Gilbert and L. Radom, *Macromolecules*, 1995, **28**, 8771; (*w*) J. P. A. Heutz, R. G. Gilbert and L. Radom, *J. Phys. Chem. A*, 1996, **100**, 18997; (*x*) L. Zhu, J. W. Bozzelli and WP. Ho, *J. Phys. Chem. A*, 1999, **103**(39), 1800; (*y*) C. J. Chen and J. W. Bozzelli, *J. Phys. Chem. A*, 2000, **104**(21), 4997.
6 (*a*) S. Roszak, R. J. Buenker, P. C. Hariharan and J. J. Kaufman, *Chem. Phys*., 1990, **147**, 13; (*b*) M. Dupuis, J. J. Wendoloski, T. Takada and W. A. Lester, *J. Chem. Phys*., 1982, **76**, 481; (*c*) K. Yamaguchi, S. Yabushita, T. Fueno, S. Kato and K. Morokuma, *Chem. Phys. Lett*., 1980, **70**, 27; (*d*) R. F. W. Bader, M. E. Stephens and R. A. Gangi, *Can. J. Chem*., 1977, **55**, 2755; (*e*) D. Wortmann-Saleh, B. Engels and S. D. Peyerimhoff, *J. Phys. Chem*., 1994, **98**, 9541.
7 (*a*) B. Engels and S. D. Peyerimhoff, *J. Phys. Chem*., 1989, **93**, 4462; (*b*) B. Engel and S. D. Peyerimhoff, *J. Phys. Chem*., 1990, **94**, 1267.
8 M. A. Teruel, R. A. Taccone and S. I. Lane, *Int. J. Chem. Kinet*., 1999, **31**(12), 867.
9 P. M. Mayer, C. J. Parkinson, D. M. Smith and L. Radom, *J. Chem. Phys*., 1998, **108**, 604.
10 M. J. Frisch, G. W. Trucks, H. B. Schlegel, G. E. Scuseria, M. A. Robb, J. R. Cheeseman, V. G. Zakrzewski, J. A. Montgomery Jr., R. E. Stratmann, J. C. Burant, S. Dapprich, J. M. Millam, A. D. Daniels, K. N. Kudin, M. C. Strain, O. Farkas, J. Tomasi, V. Barone, M. Cossi, R. Cammi, B. Mennucci, C. Pomelli, C. Adamo, S. Clifford, J. Ochterski, G. A. Petersson, P. Y. Ayala, Q. Cui, K. Morokuma, D. K. Malick, A. D. Rabuck, K. Raghavachari, J. B. Foresman, J. Cioslowski, J. V. Ortiz, B. B. Stefanov, G. Liu, A. Liashenko, P. Piskorz, I. Komaromi, R. Gomperts, R. L. Martin, D. J. Fox, T. Keith, M. A. Al-Laham, C. Y. Peng, A. Nanayakkara, C. Gonzalez, M. Challacombe, P. M. W. Gill, B. Johnson, W. Chen, M. W. Wong, J. L. Andres, C. Gonzalez, M. Head-Gordon, E. S. Replogle and J. A. Pople, *GAUSSIAN 98 (Revision A.3)*, Gaussian, Inc., Pittsburgh PA, 1998.
11 A. Nicolaides, A. Rauk, M. N. Glukhovtsev and L. Radom, *J. Phys. Chem*., 1996, **100**, 17460.
12 S. G. Lias, J. E. Bartmess, J. F. Liebman, J. L. Holmes, R. D. Levin and W. G. Mallard, *J. Phys. Chem. Ref. Data, (Suppl.)*, 1988, **1**, 17.
13 P. Y. Ayala and H. B. Schlegel, *J. Chem. Phys*., 1998, **108**, 2314.
14 J. R. Lacher and H. A. Skinner, *J. Chem. Soc. A*, 1968, 1034.
15 T. S. Papina, V. P. Kolesov and Yu. G. Golovanova, *Russ. J. Phys. Chem. (Engl. Transl.)*, 1987, **61**, 1168.
16 M. W. Chase Jr., *NIST-JANAF Themochemical Tables, Fourth Edition, J. Phys. Chem. Ref. Data, Monogr. 9*, 1998, 1–1951.
17 T. C. Ehlert, *J. Phys. Chem*., 1969, **73**, 949.
18 G. S. Lias, Z. Karpas and J. F. Liebman, *J. Am. Chem. Soc*., 1985, **107**, 6089.
19 J. A. Paulino and R. R. Squires, *J. Am. Chem. Soc*., 1991, **113**, 5573.
20 M. Born, S. Ingemann and N. M. M. Nibbering, *J. Am. Chem. Soc*., 1994, **116**, 7210.
21 E. N. Okafo and E. Whittle, *J. Chem. Soc., Faraday Trans. 1*, 1974, **70**, 1366.
22 (*a*) S. Koda, *Chem. Phys. Lett*., 1978, **55**, 353; (*b*) S. Koda, *Chem. Phys*., 1982, **66**, 383.
23 K. Rodeman, H. W. Yochims and H. Baumgartel, *J. Phys. Chem*., 1985, **89**, 3459.
24 D. W. Kohn, E. S. J. Robles, C. F. Logan and P. Chen, *J. Phys. Chem*., 1993, **97**, 4936.
25 J. J. Grabowski, in *Advances in Gas Phase Ion Chemistry*, ed. N. G. Adams and L. M. Babcock, JAI Press, Greenwich, London, 1992, p. **1**.
26 H. E. O'Neal and S. W. Benson, in *Free Radicals*, ed. J. K. Kochi, John Wiley & Sons, New York, 1973, p. 275.
27 N. N. Buravtsev, A. S. Grigor'ev and Yu. A. Kolvanovskii, *Kinet. Katal*., 1989, **30**, 449 (*Kinet. Catal. (Engl. Transl.)*, 1989, **30**, 21–30).
28 J. C. Amphlett, J. R. Dacey and G. O. Pritchard, *J. Phys. Chem*., 1971, **75**, 3024.
29 R. L. Asher, E. H. Appleman and B. J. Russic, *J. Chem. Phys*., 1996, **105**, 9781.
30 J. V. Davies and H. O. Pritchard, *J. Chem. Thermodyn*., 1972, **4**, 23.
31 A. Lord and H. O. Pritchard, *J. Chem. Thermodyn*., 1970, **2**, 187.
32 A. Lord and H. O. Pritchard, *J. Chem. Thermodyn*., 1969, **1**, 495.